

## Article

# Numerical Simulation Analysis on Hydraulic Optimization of the Integrated Pump Gate

Songbai Li <sup>1</sup>, Changrong Shen <sup>1</sup>, Tao Sun <sup>1</sup>, Li Cheng <sup>2,\*</sup>, Shuaihao Lei <sup>2</sup>, Chenzhi Xia <sup>1</sup> and Chenghua Zhang <sup>3</sup>

<sup>1</sup> The Eastern Route of South-to-North Water Diversion Project Jiangsu Water Source Co., Ltd., Nanjing 210029, China; lisongbai111@outlook.com (S.L.); shenchangrong111@outlook.com (C.S.); suntao564@outlook.com (T.S.); xiachenzhi111@outlook.com (C.X.)

<sup>2</sup> College of Hydraulic Science and Engineering, Yangzhou University, Yangzhou 214000, China; mz120190817@stu.yzu.edu.cn

<sup>3</sup> Yatai Pump & Valve Co., Ltd., Taixing 225400, China; zhangchenghua189@outlook.com

\* Correspondence: chengli@yzu.edu.cn

**Abstract:** Based on the Reynolds time mean N-S equation and standard k- $\epsilon$  turbulence model and using Computational Fluid Dynamics technology, this study aims to integrate the brake pump to carry out numerical simulation. Through the adoption of different arrangements of impending height and spacing, the hydraulic characteristics of the full tubular pump unit are analyzed. The two-dimensional streamline, velocity and pressure distribution, and three-dimensional streamline, axial velocity and vorticity distribution of the front pool of each scheme are displayed. The results show that the recommended pump installation height is  $0.8 D_d$ , the maximum limit value of the pump station design specification; in the dual-pump mode, the recommended pump spacing is  $2.00 D_s$ .

**Keywords:** integrated pump gate; full tubular pump; hydraulic characteristics; numerical simulation



**Citation:** Li, S.; Shen, C.; Sun, T.; Cheng, L.; Lei, S.; Xia, C.; Zhang, C. Numerical Simulation Analysis on Hydraulic Optimization of the Integrated Pump Gate. *Energies* **2022**, *15*, 4664. <https://doi.org/10.3390/en15134664>

Academic Editor: Helena M. Ramos

Received: 26 May 2022

Accepted: 21 June 2022

Published: 25 June 2022

**Publisher's Note:** MDPI stays neutral with regard to jurisdictional claims in published maps and institutional affiliations.



**Copyright:** © 2022 by the authors. Licensee MDPI, Basel, Switzerland. This article is an open access article distributed under the terms and conditions of the Creative Commons Attribution (CC BY) license (<https://creativecommons.org/licenses/by/4.0/>).

## 1. Introduction

Due to the rapid development of urbanization in our country and the emergence of extreme climate factors, such as after the continuous rain, in low-lying parts of the city, the water level of the inland river basin also rises, and the traditional pump station has been unable to meet the drainage function of the city. This will give our country urban pumping station flood control, a drainage function, and put forward new and higher requirements. The traditional pump sluice engineering adopts a separate arrangement of the sluice gate and pump station, but this arrangement has disadvantages such as a large occupation area, high construction cost and decentralized management of the pump sluice. The integration between the pumping station and gate station layout set up the integration of the brake pump. The pump brake characteristics include a short time limit and covers a small area; the advantages include a low operating cost, better solution to the disadvantages of traditional brake pump engineering, is especially suitable for small and medium-sized rivers of water environments and water ecology renovation projects, has a broad application foreground, and good economic and social benefits.

The integrated pump gate installs a full-flow pump on the flat gate, as shown in Figure 1. The discharge channel and the pumping channel are the same channel, which can be used not only according to the conventional gate opening and drainage, but also when the flood flow in the urban area is large and the water level of the external channel is higher than that of the internal channel, which cannot discharge the flood by self-flow; the pump starts to pump and drain the flood.

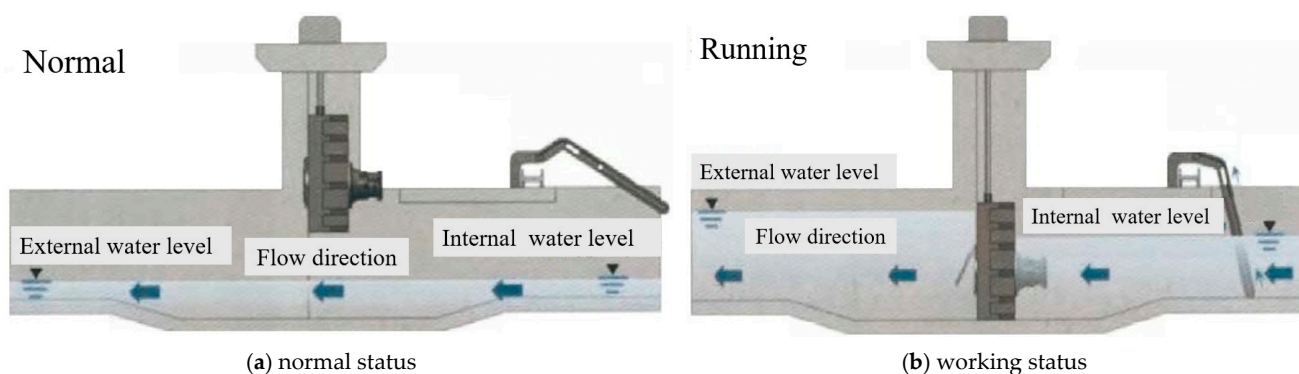


**Figure 1.** The working process of the integrated pump gate.

There are many studies on the layout of traditional sluice stations and hydraulic optimization of pump stations by domestic and foreign scholars. Luo et al. [1] used a variety of diversion pier rectification measures to improve the flow state of the front tank based on CFD calculations to improve the back flow area near the front tank divider of the gate station combined with the pump station. The results show that the diversion pier can eliminate the back flow zone in the front pool, and the numerical simulation results are verified by experiments. Feng et al. [2], aiming at the problems of back flow and deflection in the downstream of the lateral gate station project, found that the double bottom can effectively control the transverse fluctuation of the downstream water surface, shorten the range of the back flow zone, and improve the uniformity of the cross-section velocity through the method of three-dimensional numerical simulation technology and a physical model test. Gao et al. [3] studied the influence of a diversion pier on the hydraulic characteristics of the inlet pool of a gate station project based on CFD technology. The results show that a diversion pier with an appropriate length and different opening parameters can improve the hydraulic characteristics of the entrance pool of the sluice station. Wang et al. [4] used a certain gate station as the engineering background, adopted CFD numerical simulation technology, calculated and analyzed the factors affecting the inlet and outlet flow state of the gate station hub according to the single-factor analysis method, and studied the influence of the length of the diversion wall at the outlet side of the gate station and the layout of the diversion wall on the flow state. Tastan [5] found, through physical model experiments, that the strength of the vortex and the critical submerged depth are influenced by the design shape and location of the sluice inlet. Huang et al. [6] analyzed hydraulic characteristics by simulating the flow inside the inlet pool. The results showed that there is a flow singularity region under the bell mouth of the rectangular inlet pool, and a w-shaped inlet pool scheme was proposed. Tang et al. [7] used a water refill pump station in a city as the actual engineering background and analyzed the inflow flow state of the pump station under different start-up conditions based on the method of CFD numerical simulation, focusing on the improvement of the inflow flow state of the pump station using columns, grilles and water guide cones. Zi et al. [8], to eliminate vortex and wall vortex in the fore pond and inlet pond of a large pump station, found that, based on three-dimensional hydrodynamic calculation, the combined diversion pier composed of a double-l type, three-l type and cross shaped vortex elimination plate could effectively eliminate the vortex in the fore pond of the large pump station and improve the uniformity of the flow velocity distribution. Tatsuaki [9] studied how to improve the flow curvature of large water intake and the existence of a bad water intake flow pattern and set up a low-submersible diversion bridge to effectively reduce the scouring of water intake flow on other buildings on the bend, and the flow pattern was significantly improved. Wang [10], according to the traditional concrete pumping station, showed that there is a large investment, a long construction period and other existing problems based on CFD technology, researched the integration of pumping station hydraulic performance effects under different geometric parameters, studied the different pump installation locations, formed and guided the water at the

bottom of the cone geometry size effect on hydraulic performance, and accordingly put forward the optimal scheme. Echavez et al. [11] conducted a study on vortex generation on the free surface of an open intake pool through a model test. Jong et al. [12] studied the vortex under the horn pipe of the pump station inlet pool by combining a model test with numerical simulation technology and provided corresponding measures. Zhang [13] introduced, in detail, the main characteristics of the gate pump, the way of connecting the gate and the water pump, the arrangement of the gate structure, and the design specifications according to the advantages of the combination of the full penetration pump and the steel gate. To improve the hydraulic performance of the gate pump, Guo [14] studied the flow characteristics of the pump, including the flow characteristics of the pump station into the pool. Li [15] designed the traditional pump station established in the early stage with limited flood control and drainage capacity; thus, it is necessary to improve or build a new pump station with a larger water volume to solve this problem. The design and technical points of the gate body, gate pump and hoist in the integrated pump sluice are introduced in detail, which provides reference for the popularization and application of the integrated pump sluice. To sum up, there are many experimental and numerical results on the hydraulic characteristics of the traditional pump sluice at present, but there are few research results on the influencing mechanism of the hydraulic characteristics of integrated pump sluice. Shen et al. [16] analyzed the influence of the upstream and downstream water levels of the gate and the form of the submersible pump arrangement on the structural dynamic characteristics of the integrated pump gate. Shi et al. [17,18] studied the hydrostatic characteristics, hydrodynamic characteristics and flow-excited vibration characteristics of vertical and horizontal integrated pump gates using numerical simulation and model tests.

In summary, there are more experimental and numerical calculation results on the hydraulic characteristics of the traditional gate station type combined pumping stations, but there are fewer studies on integrated pump gates, and most of them are about the static dynamic characteristics of gate structures, while there are fewer research results on the mechanism of the influence of hydraulic characteristics. Therefore, it is important to carry out the key technologies of hydraulic and structural optimization of integrated pump gates to improve the efficient and stable operation of integrated pump gates in combination with Chinese pump station design codes [19].

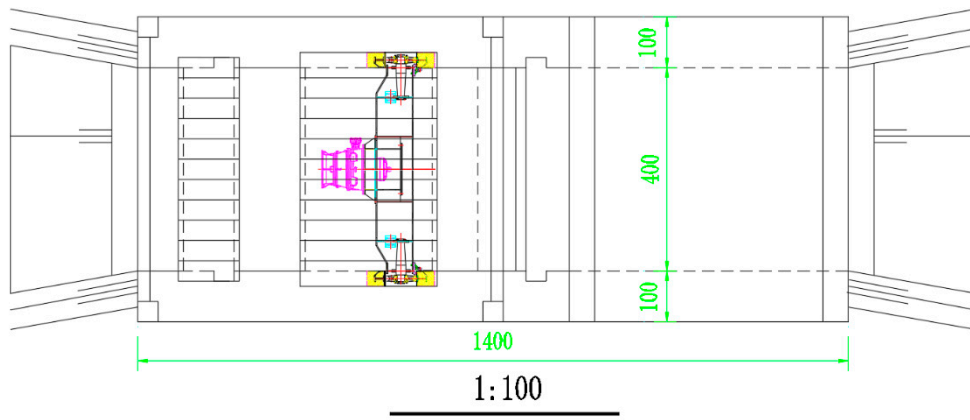
## 2. Computational Model and Numerical Simulation

### 2.1. Project Overview

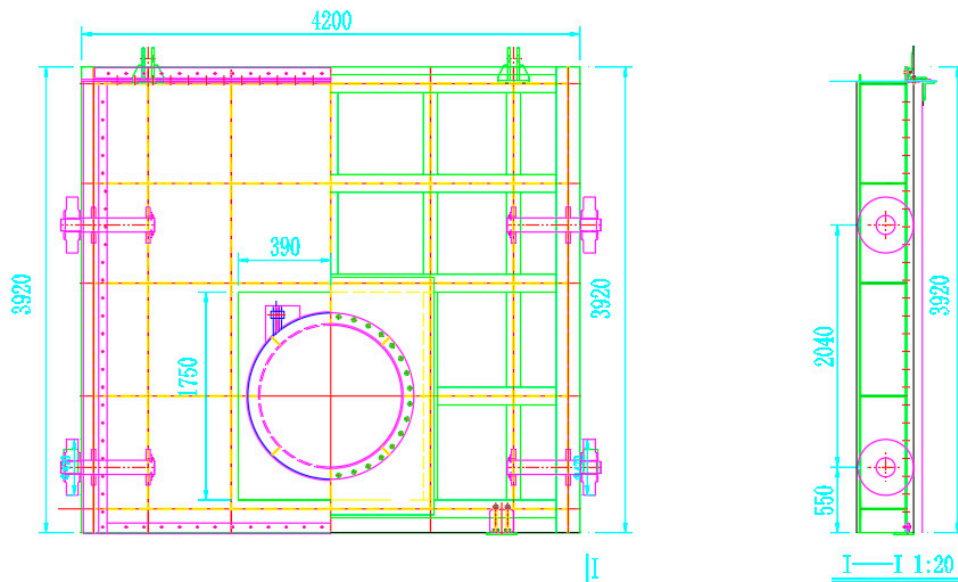
A city adopts a new integrated pump gate, which adopts a full tubular pump. The plane size of the pump room is 4.0 m × 14.0 m. The pump unit adopts horizontal installation; the inlet flow is 1.1 m<sup>3</sup>/s, and the outlet pipe diameter is DN 700 mm. The plane layout and gate size structure of the integrated pump sluice are shown in Figure 2, where I-I section is the side view of the gate.

### 2.2. Calculation Model and Control Parameter

The calculation model of the integrated pump gate is built in UG 12.0 software. We choose the diameter of the impeller:  $D = 600$  mm, the diameter of inlet horn is 750 mm, the diameter of inlet is 700 mm, the number of impeller blades and guide vanes are 3 and 7, respectively, the design head of the inlet side is 3.8 m, the level of lowest water is 3.5 m, the design head of the outlet side is 4.8 m, the base plate elevation is 1.0 m, and the calculation model of the integrated pump gate and full flow channel is shown as Figure 3.



(a) Schematic diagram of the layout structure of the integrated pump gate in a certain area (unit: cm)



(b) Schematic diagram of the structure and dimensions of the integrated pump gate (unit: mm)

**Figure 2.** Schematic diagram of the plane layout of the integrated pump gate and the size and structure of the gate.

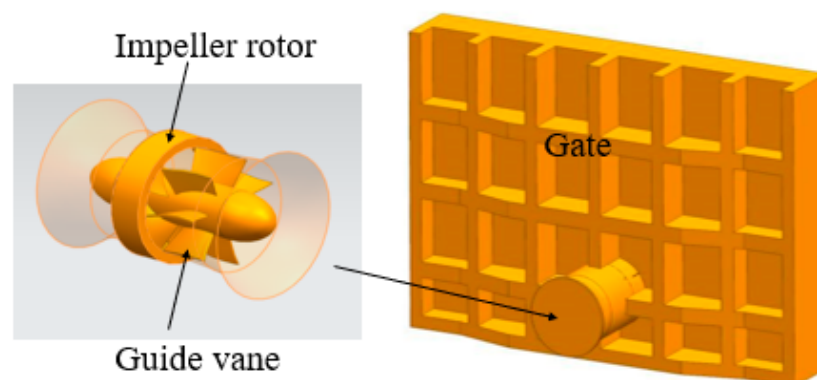


**Figure 3.** Calculation model of the integrated pump gate full flow channel.

### 2.3. Control Equations

The flow of water in the integrated pump gate is a complex three-dimensional turbulent flow, and the water body can be regarded as an incompressible fluid that obeys the law of conservation of mass, the law of conservation of energy and the law of conservation of momentum. The operation of the pump can ignore the heat transfer factor, so the energy equation is not considered. The control equations include the continuity equation and the momentum equation, which is also known as the *N-S* (Navier–Stokes) equation, with the following equation expressions:

$$\frac{\partial \rho}{\partial t} + \nabla(\rho u) = 0, \quad (1)$$

Momentum equation:

$$\frac{\partial(\rho u)}{\partial t} + \nabla(\rho uu - \tau) = F, \quad (2)$$

### 2.4. Calculation Method and Turbulence Model

The numerical simulation methods of turbulence can usually be divided into three categories: direct numerical simulation, Reynolds averaged simulation and large eddy simulation. The Reynolds averaged simulation method (RANS) refers to the Reynolds averaging the physical quantities of the flow field in the time domain and then solving the resulting time-homogenized control equations. This method is computationally efficient, with early applications in engineering. The commonly used RANS models include the Spalart–Allmaras model, *k-ε* model and *k-ω* model. This is the most widely used numerical simulation method for turbulence in the field of pumps and pumping stations.

$$\frac{\partial(\rho k)}{\partial t} + \frac{\partial(\rho k u_i)}{\partial x_i} = \frac{\partial}{\partial x_j} \left[ \left( \mu + \frac{\mu_t}{\sigma_k} \right) \frac{\partial k}{\partial x_j} \right] + G_k + G_b - \rho \varepsilon + S_k, \quad (3)$$

$$\frac{\partial(\rho \varepsilon)}{\partial t} + \frac{\partial(\rho \varepsilon u_i)}{\partial x_i} = \frac{\partial}{\partial x_j} \left[ \left( \mu + \frac{\mu_t}{\sigma_\varepsilon} \right) \frac{\partial \varepsilon}{\partial x_j} \right] + G_{1\varepsilon} \frac{\varepsilon}{k} (G_k + G_{3\varepsilon} G_b) - G_{2\varepsilon} \rho \frac{\varepsilon^2}{k} + S_\varepsilon, \quad (4)$$

Numerous calculations have shown that the model can be better used to simulate some of the more complex flows in pumping stations. Therefore, in this paper, based on a Reynolds averaged *N-S* control equation and standard *k-ε* turbulence model, numerical simulation analysis and hydraulic optimization design study of the full flow channel of an integrated pump gate are carried out.

### 2.5. Boundary Conditions

The inlet condition of the integrated pump gate is set as mass flow, and the medium intensity is 5%; the outlet of the integrated pump gate is set as pressure discharge. The impeller part is set as 730 r/min. Ignoring the heat exchange and heat conduction between the front pool liquid surface and air, the liquid surface is assumed to be a rigid-lid hypothesis, and the free surface is assumed to be a free boundary condition. The solid boundary of the calculation area is set as a wall boundary condition, and the standard wall function is adopted at the solid wall, which is set as a non-slip boundary condition (the velocity components in *x*, *y*, *z* directions are 0); the first-order upwind scheme is adopted, and the convergence accuracy is  $10^{-4}$ . To ensure the continuity of the interface, the static and dynamic interfaces adopt the frozen stator model.

### 2.6. Mesh Generation

The mesh is the basis for the spatial discretization of the control equations. The computational domain is divided into 6 parts: forebay, inlet sump, water guide cone, impeller, guide vane, and outlet sump. The grid dissection of the computational domain is performed using a blocking strategy. Hexahedral meshing of the impeller and guide vane uses ANSYS turbo grid software. Hexahedral meshing of forebay, inlet sump, water guide

cone and outlet sump is done by ICEM software. Finally, each part of the mesh model is assembled in CFX, as shown in Figure 4.

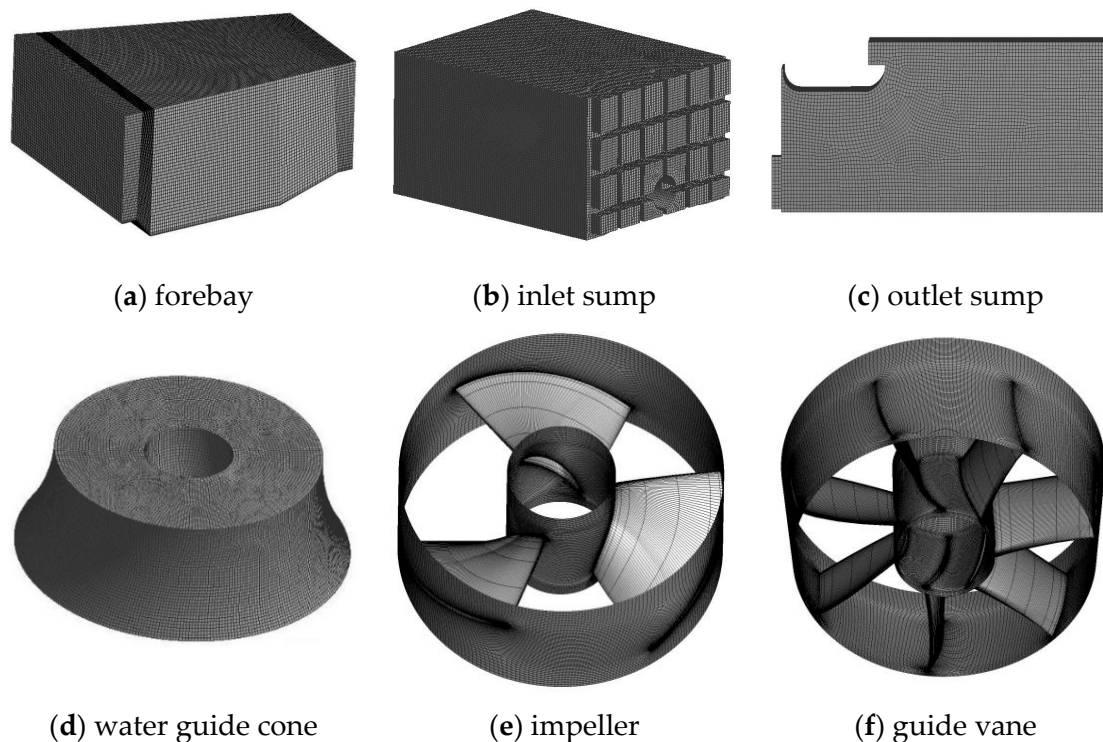


**Figure 4.** Computational grid diagram.

The independency of the number of control grids in 10 million, 20 million, 30 million, 40 million, 50 million, 60 million, 70 million, 90 million, 110 million, 130 million, and 150 million regions of the inflow site in the sluice station construction project is analyzed, and the analysis of grid independence is based on the difference of device efficiency under different grid number schemes. Figure 5 shows the grid independence verification. With an increase in the number of grids, the efficiency of the device shows an upward trend. When the number of grids in the inlet part of the pump gate reaches 110 million, the increased value of the efficiency value decreases significantly and gradually becomes stable. It is finally determined that the number of grids in the inlet part of the pump gate is 110 million, and the overall grid number is 218 million. The number of grid nodes and the grid numbers of each computing component are shown in Table 1.

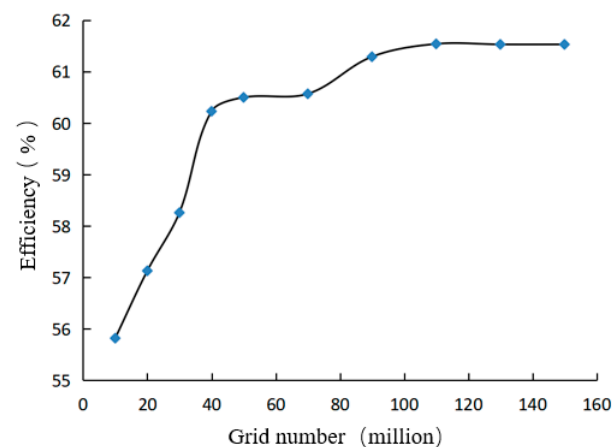


**Figure 5.** Grid independence.

**Table 1.** The number of grids and nodes in each computing part.

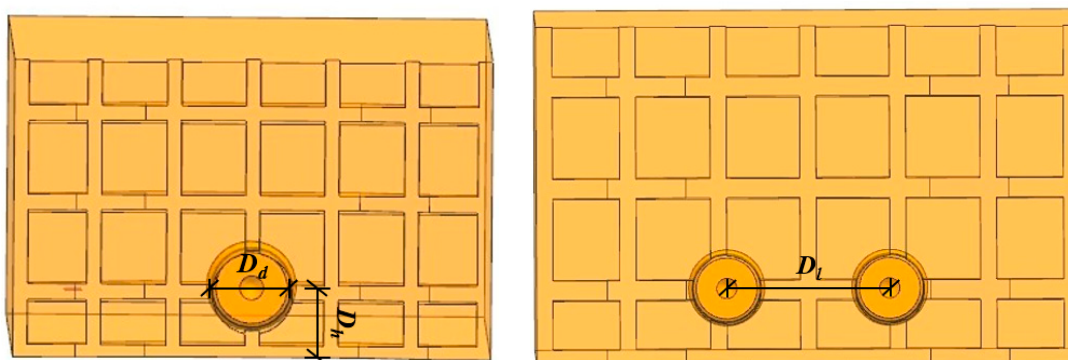
Computing Part	Number of Nodes	Grid Numbers
Forebay	308,334	324,000
Inlet sump	474,120	449,000
Forward water guide cone	233,652	275,182
Impeller	352,584	320,232
Guide vane	492,646	437,710
Behind water guide cone	103,660	121,990
Outlet sump	247,937	257,047

### 2.7. Scheme Design

The different water pump suspension heights and arrangement spacings of the re-search plans are shown in Table 2. In single pump mode, the heights are selected as  $0.6 D_d$ ,  $0.8 D_d$ ,  $1.7 D_d$ , and  $2.6 D_d$ . In the dual-pump mode, with a water pump suspended height of  $0.8 D_d$  as the benchmark, the arrangement spacings are selected as  $1.0 D_s$ ,  $1.5 D_s$ ,  $2.0 D_s$ , and  $2.33 D_s$ . Figure 6 is a schematic diagram of the suspended height and arrangement spacing of the new integrated pump gate.

**Table 2.** Research schemes of different suspended heights.

Scheme	Suspension Height ( $D_h/D_d$ )	Arrangement Spacing ( $D_l/D_s$ )	Remark
1	0.6	—	single pump
2	0.8	—	
3	1.7	—	
4	2.6	—	
5	0.8	1.00	double pumps
6	0.8	1.50	
7	0.8	2.00	
8	0.8	2.33	

**Figure 6.** Chart of suspended height and layout distance of the new integrated pump gate.

## 3. Result Analysis

### 3.1. Selection of Characteristic Sections and Axes

Ten characteristic sections and five characteristic axes are selected for qualitative and quantitative analysis of the hydraulic performance of the integrated pump gate inlet sump under different schemes, as shown in Figure 7.

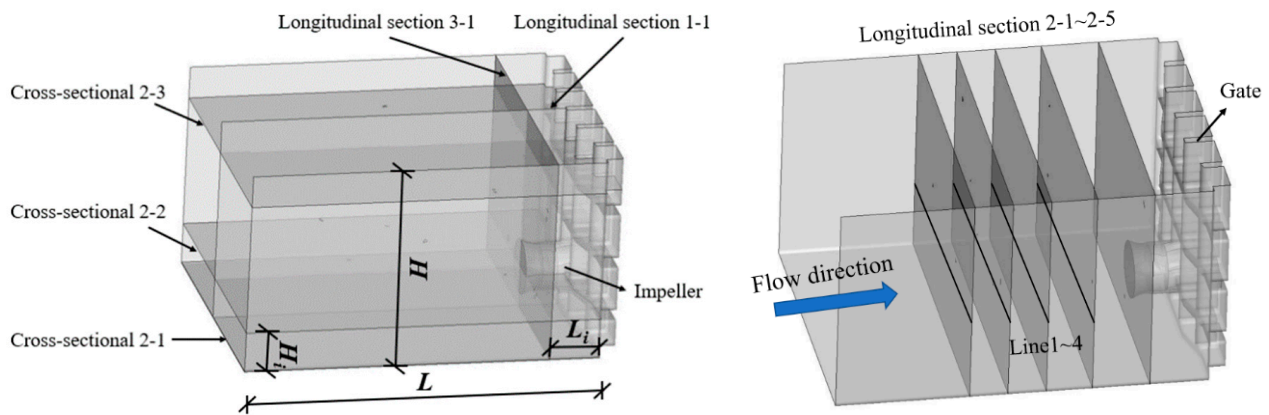


**Figure 7.** Schematic diagram of the selection of feature sections and axis positions.

### 3.2. Analysis Parameters

Axial flow uniformity can represent the uniform characteristics of the flow velocity on the characteristic section. The larger the value, the more uniform the axial velocity distribution. The calculation formula is as follows:

$$V_u = \left( 1 - \frac{1}{V_a} \sqrt{\frac{\sum (u_{ai} - u_a)^2}{n}} \right) \times 100, \quad (5)$$

The mechanical energy loss caused by friction and impact between the selected sections due to the presence of water flow and solid boundaries is expressed by hydraulic loss, and the smaller the value, the smaller the mechanical energy lost between the sections, i.e., the smaller the hydraulic loss. The calculation formula is as follows:

$$h = \Delta p / \rho g, \quad (6)$$

What can be obtained by numerical simulation is the flow velocity field and pressure field, and the head of the pump unit can be calculated with the help of Bernoulli's energy equation.

$$H_s = \frac{P_{inlet} - P_{outlet}}{\rho g}, \quad (7)$$

By integrating the values to calculate the torque generated when interacting on the impeller, the efficiency of the pumping unit can be predicted.

$$\eta = \frac{\rho g Q H_s}{T \omega}, \quad (8)$$

### 3.3. Analysis of Suspended Height Results

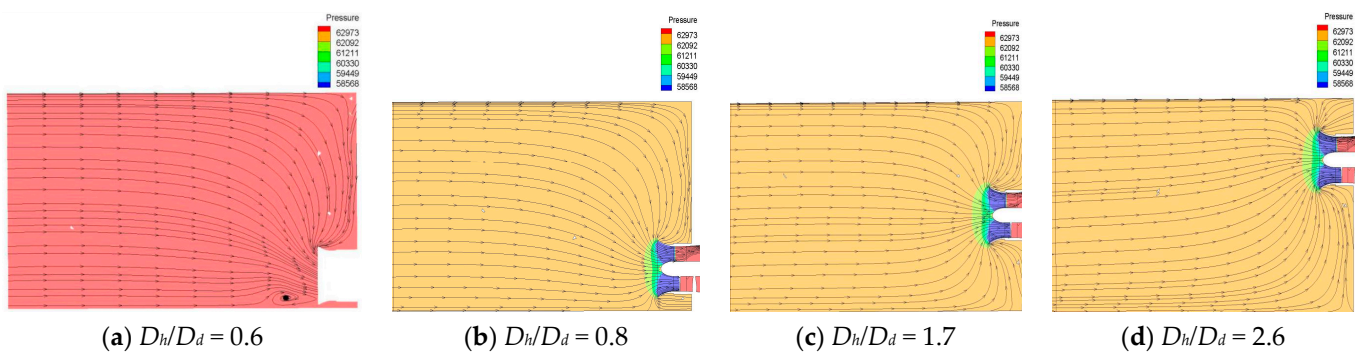
Table 3 shows the CFD performance of the integrated pump gate under different suspended heights. With the increase of the pump suspension height, the pump head appears to rise significantly in plan 3. The head does not change significantly in other schemes, but with the pump installation position increasing, the efficiency of the device obviously shows a rising trend.

Figure 8 shows the pressure and flow distribution at inlet pool section 1-1. As can be seen from the figure, when the pump installation suspended height is  $0.6 D_d$ , the overall pressure distribution is more uniform, the pump installation height and into the pool at the bottom of the distance is closer, affecting the flow of water into the pump unit flow pattern in the bottom of the flared pipe in front of the bottom of a whirlpool. When the pump installation suspended height is  $0.8 D_d$ , the into the pool overall pressure distribution is more uniform, but in the flared pipe inlet near the pressure change, it is not very different, slightly lower, and in the surface flow line through the gate panel

flow to the flared pipe inlet, the overall flow line distribution is more regular. When the pump installation suspended height is  $1.7 D_d$ , the overall pressure and streamline distribution is not significantly different from scheme 9, and the streamline distribution is more symmetrical up and down; when the pump installation suspended height is  $2.6 D_d$ , the water streamline flows from the bottom to the top.

**Table 3.** CFD performance of each suspended height research program.

Plan	Design Water Level (m)	Head (m)	Efficiency (%)
1	3.8	3.920	53.39
2	3.8	3.930	56.19
3	3.8	3.962	58.26
4	3.8	3.922	62.46



**Figure 8.** Suction sump pressure and flow line diagram (section 1-1, unit:pa).

Figure 9 shows the pressure and flow line distribution at the inlet pool in section 2-1. When the pump installation suspended height is  $0.60 D_d$ , it can be seen from the figure that the pressure distribution of the section at the mouth of the flared pipe is uniform, and the flow line forms a vortex point at the center of the flared pipe, the swirl degree is relatively poor, and the distribution of the flow line is poor; when the pump installation suspended height is  $0.8 D_d$ , the pressure of the section changes, and the pressure near the mouth of the flared pipe decreases and then increases. In schemes 3 and 4, the pressure distribution is more consistent with scheme 2, and the flow line distribution in scheme 3 is more uniform, and there is no obvious back swirl at the center of the flow line.

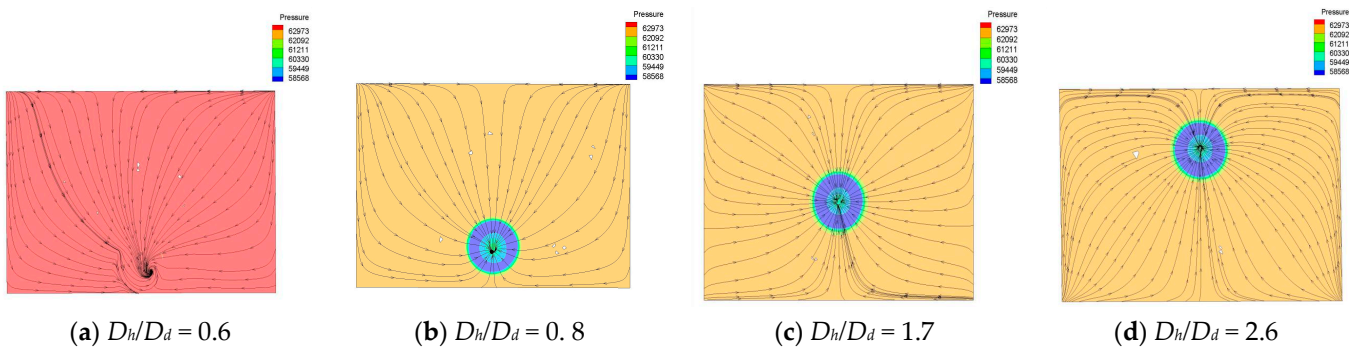


**Figure 9.** Suction sump flow line and pressure distribution diagram (section 3-1, unit:pa).

Figure 10 shows the flow line and pressure distribution diagram of inlet pool section 2-2. As can be seen from the figure, when the pump installation suspended height of  $0.6 D_d$ , the area near the mouth of the flared pipe appeared a number of vortices, and there is a slightly larger range of negative axial velocity distribution area at the location of the vortex. When the pump installation suspended height is  $0.8 D_d$ , the flow line gathered in front is more obvious, and the flow line is gathered at the back of a smaller area of

negative direction axial velocity distribution area. When the pump installation suspended height is  $1.7 D_d$ , the water flow line is obviously gathered at the gate panel, and there is a convergence point in the center of the inlet pool area, and the axial flow velocity increases slightly near the gate panel. When the suspended height of the pump installation is  $2.6 D_d$ , the water flow line is gathered near the gate, and the axial flow velocity increases at the gate panel.

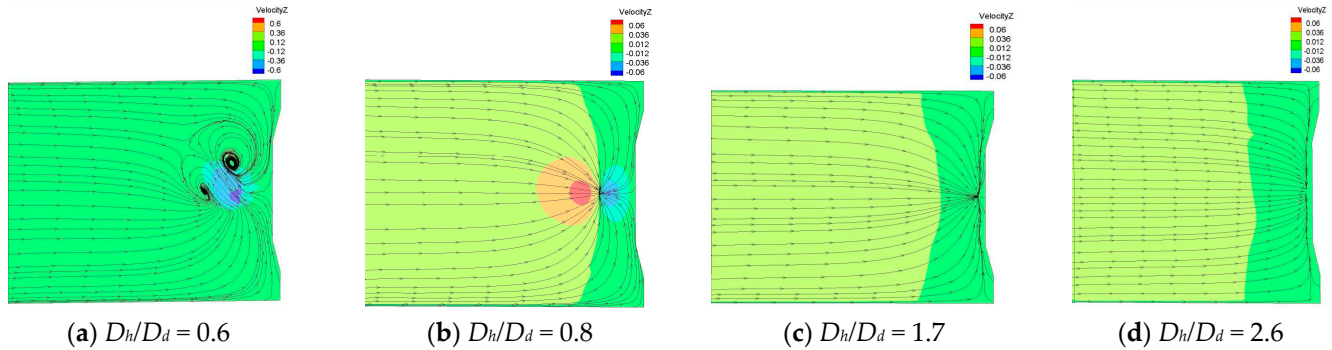


Figure 10. Suction sump flow line and axial flow velocity distribution (section 2-2, unit m/s).

Figure 11 shows the flow line and flow velocity distribution of the inlet pool section 2-2. As can be seen from the figure, when the pump installation suspended height of  $0.6 D_d$ , the flared pipe mouth into the water is in front of a larger axial velocity distribution area and the flared pipe mouth side wall is behind a little reverse axial velocity distribution in the direction of the water into the right side of the flared pipe mouth side wall at the obvious small whirlpool. When the pump installation suspended height is  $0.8 D_d$ , the into the pool axial velocity distribution is larger and the flared pipe mouth into the water axial velocity distribution. When the suspended height of the pump is  $1.7 D_d$ , the axial velocity distribution of the inlet water is more consistent with scheme 8, the flow lines converge at one point at this section, and the axial velocity distribution in the negative direction is not obvious. When the suspended height of the pump is  $2.6 D_d$ , the flow lines at this section converge uniformly near the gate panel as a whole. The axial velocity distribution is lower, as it is closer to the gate panel, and there is no reverse axial velocity region distribution.

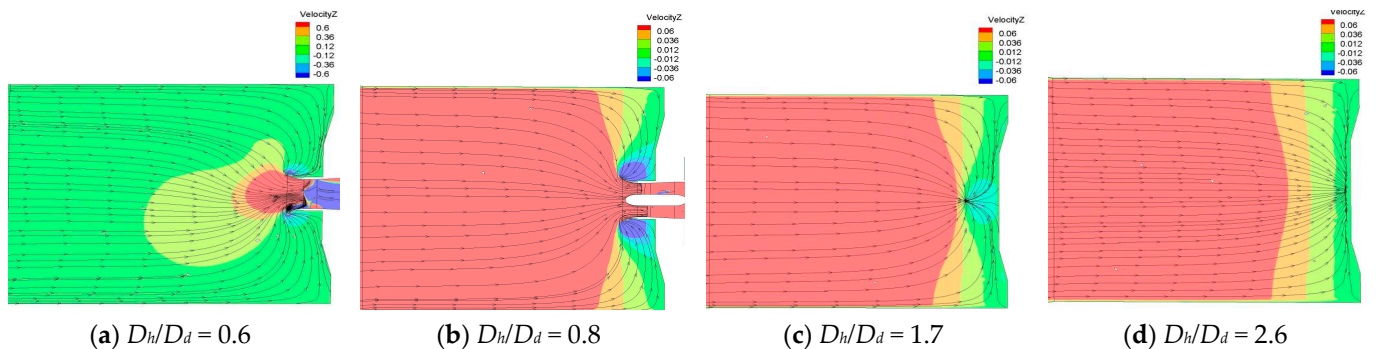


Figure 11. Suction sump flow line and axial flow velocity distribution (section 2-2, unit: m/s).

Figure 12 shows pool section 2-3 flow line and flow velocity distribution diagram. As can be seen from the figure, when the pump installation suspended height is  $0.6 D_d$ , the into the pool overall axial velocity distribution is small, the overall flow line is more uniformly gathered in the front side of the gate panel, and there is no larger vortex. When the pump installation suspended height is  $0.8 D_d$ , into the pool before the flared pipe mouth axial velocity is larger, but the distance from the flared pipe mouth increases, the axial velocity gradually decreases, and the flow line is gathered in the gate panel at the side wall; there is

no obvious streamline vortex, and the streamline collection on both sides of the inlet pool is not obvious. When the pump installation suspended height is  $1.7 D_d$ , the larger axial flow velocity distribution area increases, and the streamline collection is more obvious than program 8, and basically concentrated in the front side of the gate panel. When the pump installation suspended height is  $2.6 D_d$ , the larger axial flow velocity distribution has been extended to the streamline collection area.

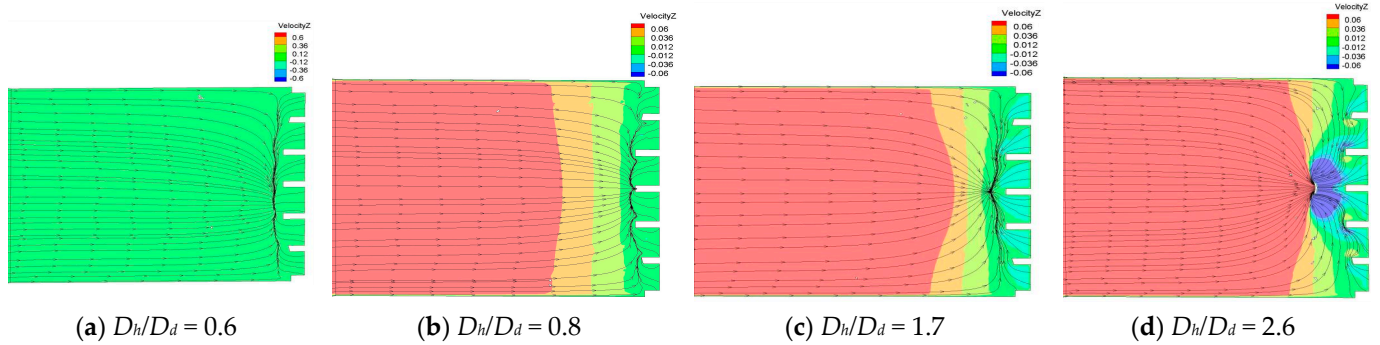


Figure 12. Suction sump flow line and axial flow velocity distribution (section 2-3, unit: m/s).

Figure 13 shows the axial velocity distribution of the different sections of the inlet sump. It can be seen from the figure that when the pump installation suspended height is  $0.6 D_d$ , section 2-4 has the more obvious axial velocity distribution differences and a small range of reverse axial velocity distribution in the right side of the inlet direction. When the pump installation suspended height is  $0.8 D_d$ , section 2-4 in the reverse direction of the axial velocity distribution area disappears, but the relative position of the flared pipe mouth at the larger axial velocity on the bottom of the inlet pool is obvious. When the suspended height of the pump installation is  $1.7 D_d$ , the larger axial velocity distribution area at the relative position of the flared pipe mouth in section 2-4 is reduced, and the overall axial velocity distribution is more uniform. When the suspended height of the pump installation is  $2.6 D_d$ , a smaller range of axial velocity increase area starts to appear at the surface layer in section 2-3, and section 2-5 obviously shows that the larger axial velocity has a greater impact on the surface layer.

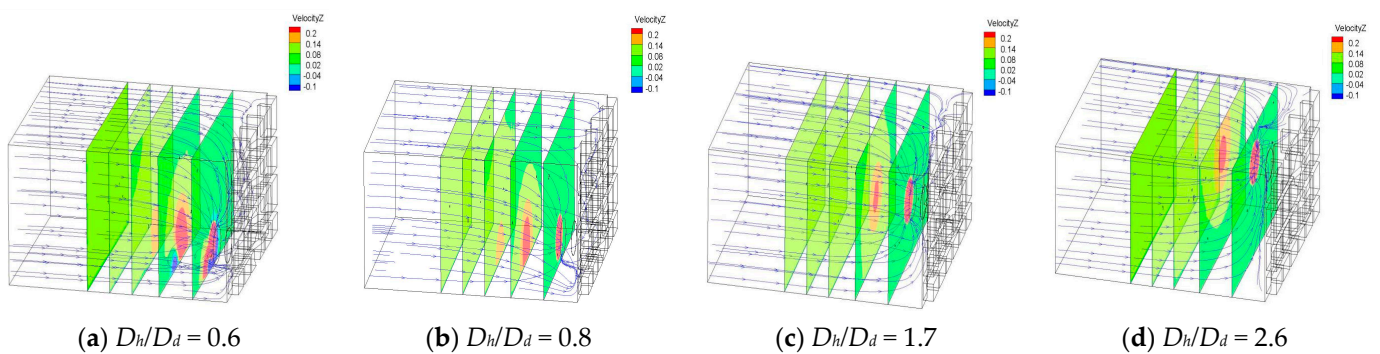


Figure 13. Suction sump of different sections of the axial flow velocity distribution (sections 2-1~2-5, unit: m/s).

Figure 14 shows a three-dimensional vortex volume diagram of the inlet sump. When the suspended height of the pump is  $1.7 D_d$ , the vortex distribution at the bottom of the gate becomes shorter and symmetrically distributed to the left and right, and the vortex disappears in the area below the flared mouth. When the suspended height of the pump is  $2.6 D_d$ , the overall vortex distribution is still concentrated in front of the flared mouth, and the vortex disappears at the bottom of the gate.

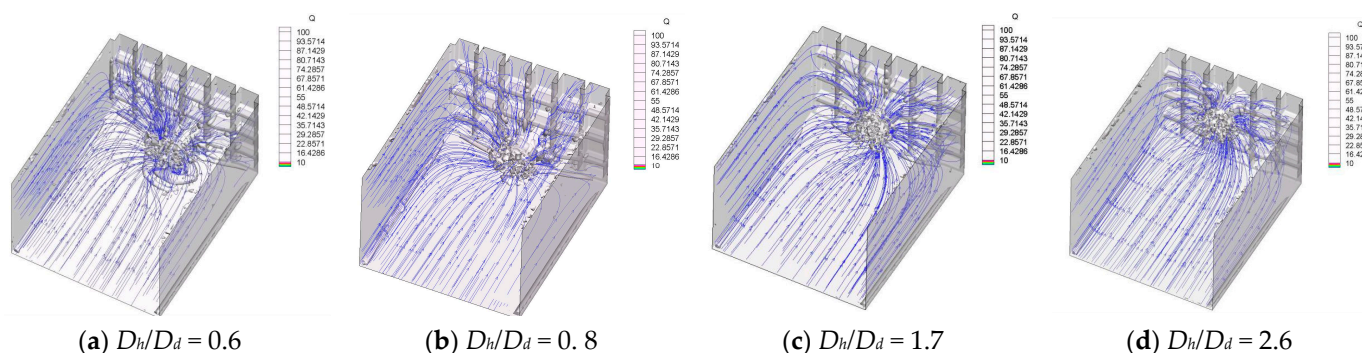


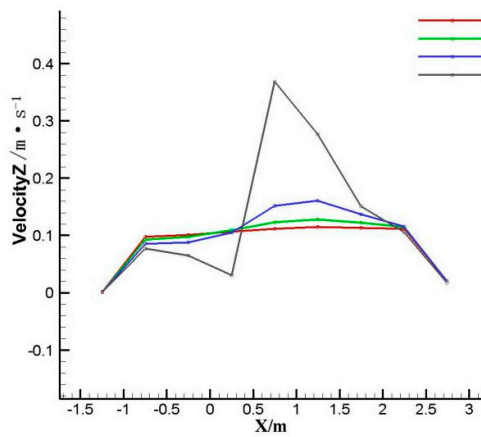
Figure 14. Suction sump three-dimensional vorticity diagram (unit: $s^{-1}$ ).

Table 4 shows the CFD performance of each study scheme under different suspended heights. According to the data in the graph, it can be seen that the axial flow velocity distribution at section 3-1 in design scheme 1 is obviously low, and the loss to the hydraulic force is relatively large. In scheme 2, the uniformity of axial flow velocity at section 2-3 is 64.25%, and the partial loss to the hydraulic force at the inlet to section is relatively small. In design scheme 3, the uniformity of axial flow velocity at section 2-3 is significantly improved with the increase of the installation height of the suspended pump, and the loss to the partial hydraulic force is also aggravated. In scheme 4, with the further deepening and increasing of the installation height of the suspended pump, the uniformity of the axial flow velocity in section 2-3 showed a very substantial decrease, with a rate of decrease close to 10%, and the partial hydraulic loss did not change significantly.

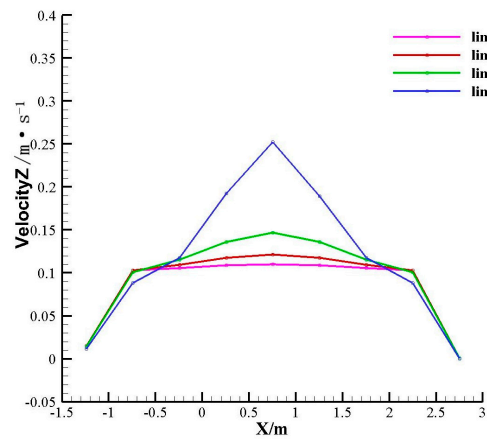
Table 4. CFD performance of the research program.

Plan	Discharge Q ( $m^3/s$ )	Inlet Side Water Level (m)	Section 2-3 Axial Flow Rate Uniformity (%)
1	1.1	3.8	56.72
2	1.1	3.8	64.25
3	1.1	3.8	70.51
4	1.1	3.8	60.66

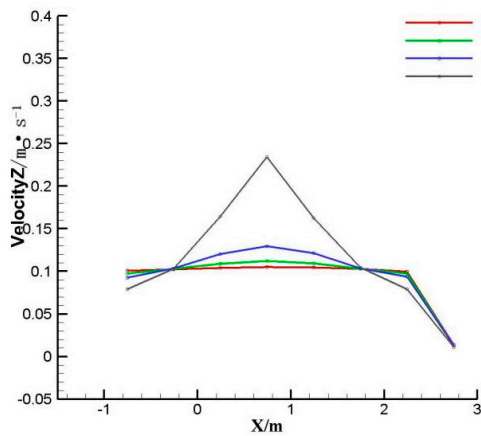
Figure 15 shows the axial flow velocity distribution on different axes under different suspended installation heights. It can be seen from the figure that when the suspended installation height of the pump is  $0.6 D_d$ , the axial flow velocity distribution is uneven, and the axial flow velocity distribution on the line4 axis can be seen obviously. When the suspended installation height of the pump is  $0.8 D_d$ , there is no obvious change in the axial flow velocity on the line 1–3 axes, and the axial flow velocity distribution is better. The axial velocity distribution in the center of the line4 axis is obviously improved; with the continuous improvement of the pump installation position, the overall axial velocity distribution is not much different from the axial velocity distribution under scheme 2.



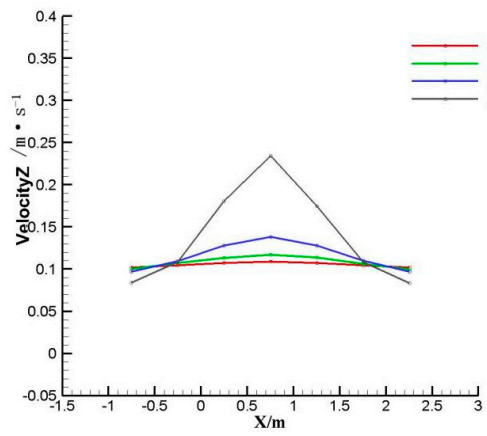
(a)  $D_h/D_d = 0.6$



(b)  $D_h/D_d = 0.8$



(c)  $D_h/D_d = 1.7$



(d)  $D_h/D_d = 2.6$

**Figure 15.** Suction sump multi-axis on the axial flow velocity distribution with different overhang heights.

### 3.4. Layout Distance Results Analysis

Figure 16 shows the 1–1 pressure and flow line distribution diagram for the suction sump. As can be seen from the figure, when the distance of the pump is  $1.00 D_s$ , the suction sump and the bottom of the gate panel appear to have a larger pressure area. When the pump distance is  $1.50 D_s$ , larger pressure distribution area of the suction sump and the bottom of the gate panel is obviously reduced. When the pump distance is  $2.00 D_s$ , the overall pressure distribution in the suction sump appears uneven, and the pressure of the suction sump inlet is reduced. With streamline convergence into the sump near the bottom of the front of the gate panel, the water flow convergence area appears to have a pressure increase area. When the pump spacing is  $2.33 D_s$ , the water flow convergence area appears to have a further expanded pressure increase.

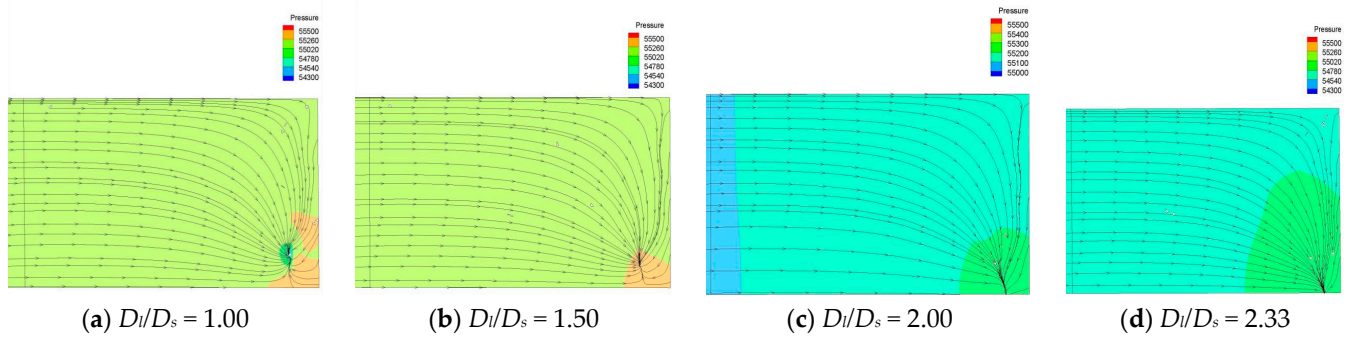


Figure 16. Suction sump pressure and flow line distribution (section 1-1, unit: pa).

Figure 17 shows the pressure and flow line distribution of the suction sump section 3-1. As can be seen from the figure, when the distance of the pump is  $1.00 D_s$ , the bottom of the suction sump below the flared pipe mouth appears to have a significantly larger range in the pressure increase area. In program 6, the pressure distribution relative to the larger area pump range has been reduced, as shown in the pressure distribution area between the two pumps is larger. In program 7, the overall pressure distribution of the suction sump significantly decreased, and the overall flow line distribution is better; with the increase of the pump center distance, the pressure at the bottom of the suction sump between the two pumps showed an overall increase of diffusion distribution.

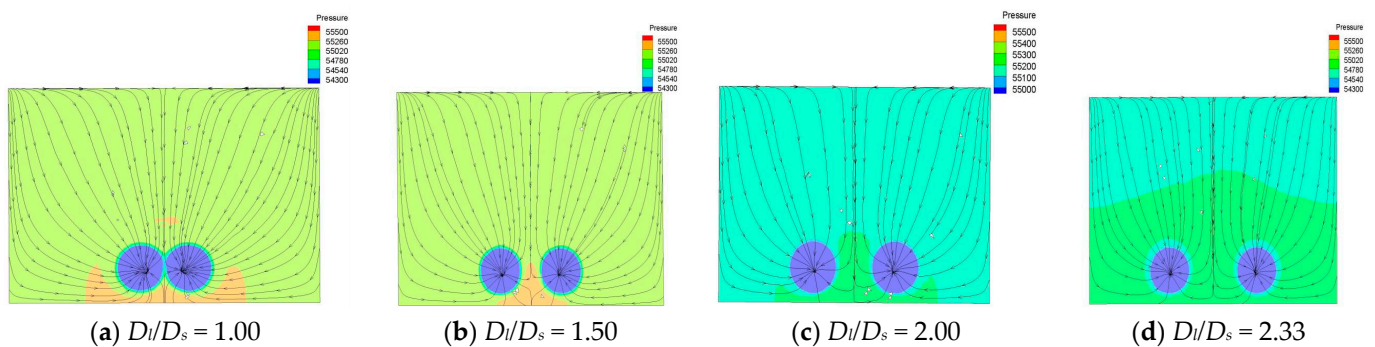


Figure 17. Suction sump pressure and flow line distribution (section 3-1, unit: pa).

Figure 18 shows the suction sump section 2-1 axial flow velocity and flow line diagram. As can be seen from the figure, when the distance of pump is  $1.00 D_s$ , the axial flow velocity distribution in front of the flared pipe mouth is larger overall, behind the flared pipe mouth appears a significantly larger area of reverse direction axial flow velocity distribution, and water flow lines converge into one place. In program 6, with the increase in the distance between the two pumps, the overall reverse direction axial flow velocity distribution behind the flared pipe mouth presents two pieces of left and right symmetric distribution, and water flow lines converge into two places. In program 7, the axial flow distribution is in the opposite direction behind the flared mouth; with the further increase of the distance between the pump centers, the area of the axial flow distribution in the opposite direction behind the flared mouth disappears obviously, and the curvature of the flow line between the two pumps increases obviously.

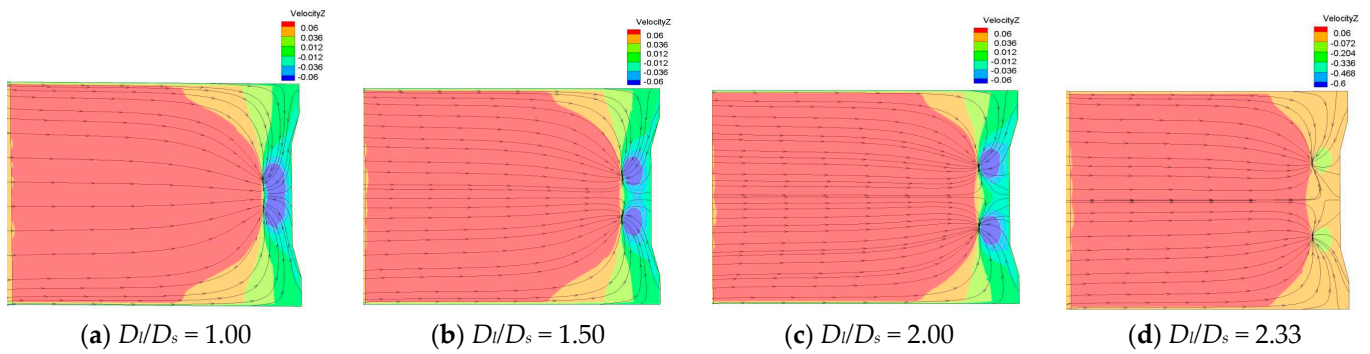


Figure 18. Suction sump axial flow velocity and flow line diagram (section 2-1, m/s).

Figure 19 shows the axial flow velocity and flow line diagram of suction sump section 2-2. As can be seen from the figure, in programs 5 and 6, the two pumps flared pipe mouth goes into the water side wall near the gate, and there is an obvious reverse direction axial flow velocity distribution between the two pumps. In program 7, the reverse direction axial flow velocity distribution region between the two pumps appears separated; with the further increase in the pump center distance, in program 8, the reverse direction axial flow velocity distribution region obviously disappears.

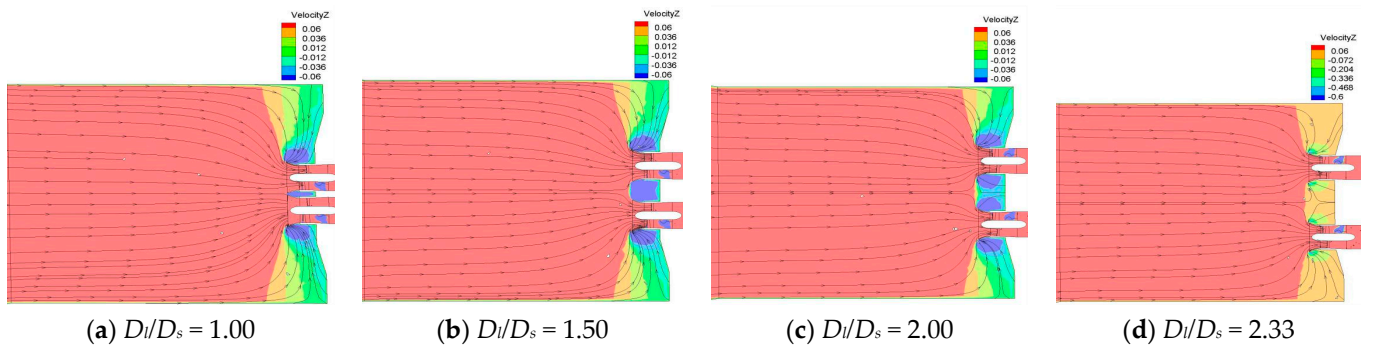


Figure 19. Suction sump axial flow velocity and flow line diagram (section 2-2, unit: m/s).

Figure 20 shows the axial flow velocity and flow line diagram of the suction sump section 2-3. As can be seen from the figure, in programs 5–8, the pressure as a whole presents a step distribution, from the inlet of the suction sump to the gate panel, the pressure distribution gradually shrinks, and finally presents the reverse direction distribution. In program 8, the overall pressure distribution presents two areas, the gate recess does not appear in the reverse axial flow velocity distribution, and the flow line is no longer neatly distributed.

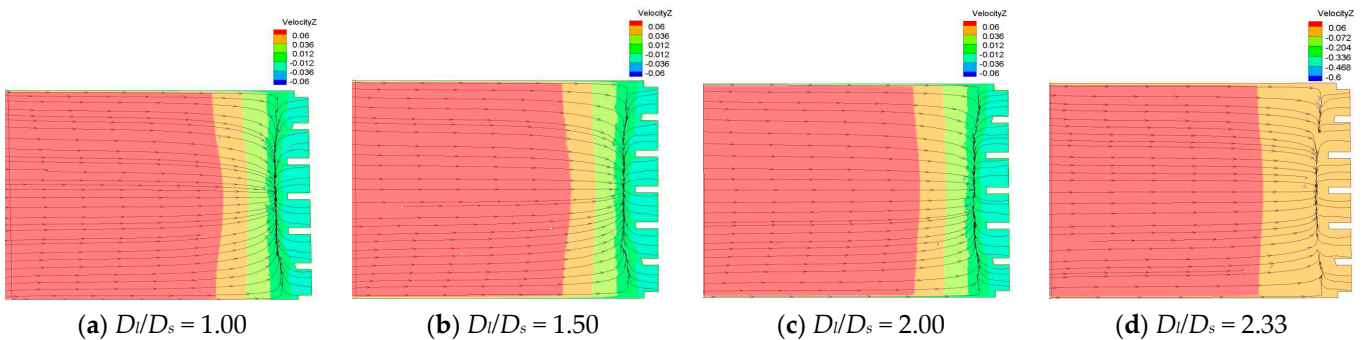


Figure 20. Suction sump axial flow velocity and flow line diagram (section 2-3, unit: m/s).

Figure 21 shows the axial flow velocity and flow line diagram of suction sump section 2-2. As can be seen from the figure, in programs 5–8, the overall axial flow velocity distribution is not significantly different. From the surface layer of section 2-1, the overall axial flow velocity began to gradually decline. In addition to the flared pipe mouth of section 2-5 at the relative location, the other areas of relative axial flow velocity distribution are smaller.

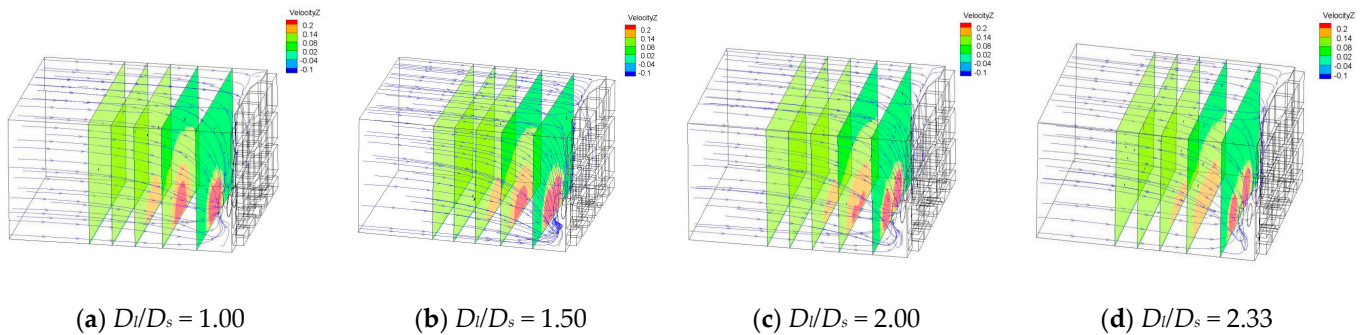


Figure 21. Suction sump of different sections of axial flow velocity distribution cloud (sections 2-1~2-5, unit: m/s).

Figure 22 shows the three-dimensional vortex map with different pump distances. As can be seen from the figure, in program 5, the vortex distribution before the pressure flared mouth is more concentrated, and the vortex below the flared mouth has an obvious vortex mass distribution; with the increasing pump distance, the vortex distribution before the flared mouth as a whole has no obvious difference, and the distribution is denser, but with the increasing distance, the vortex is no longer distributed in mass.

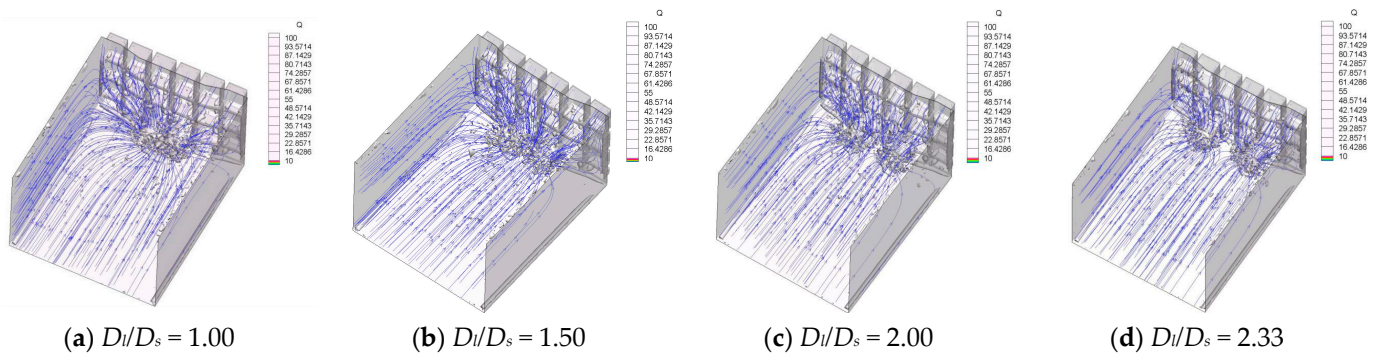


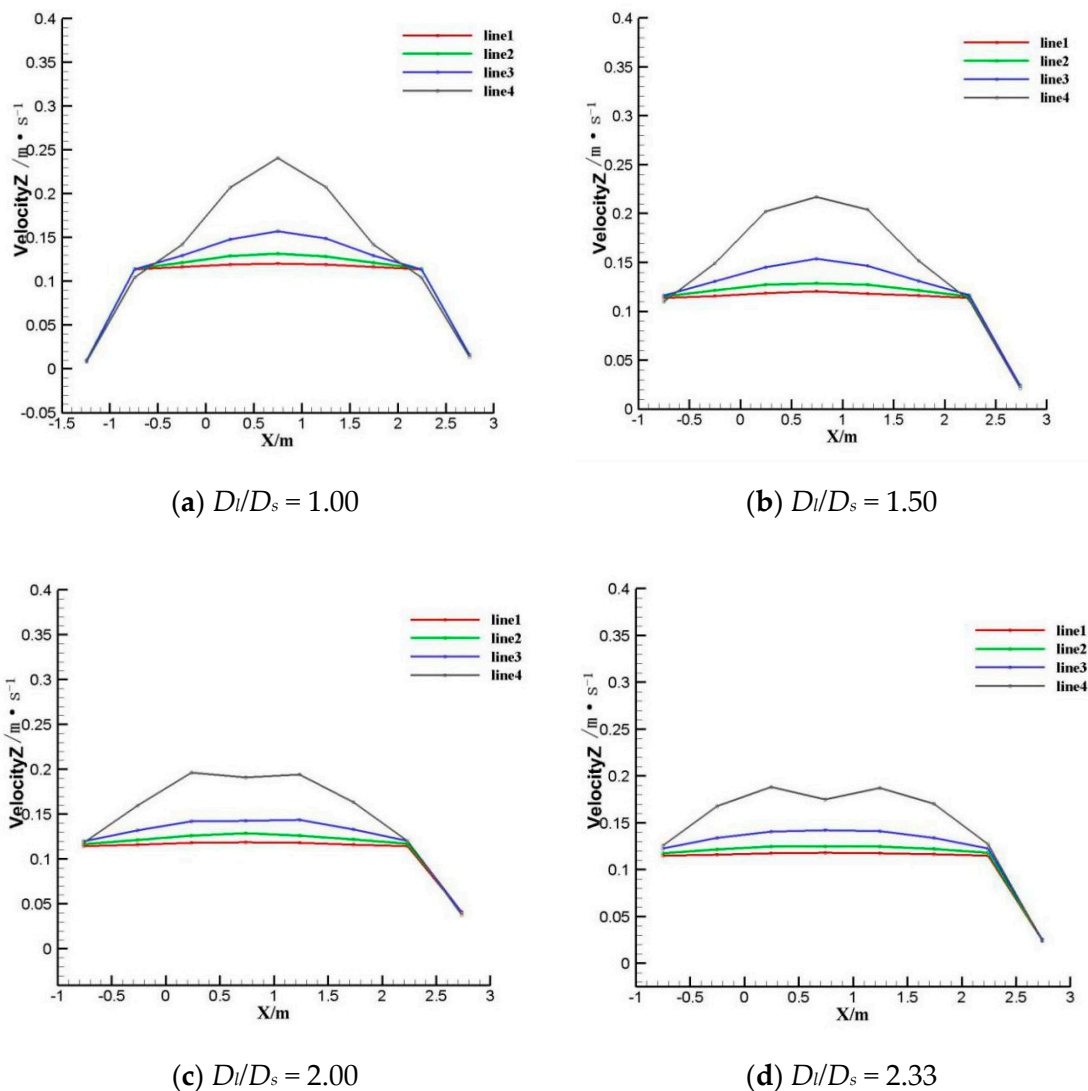
Figure 22. Suction sump three-dimensional vortex map (unit: s<sup>-1</sup>).

Table 5 shows the CFD performance analysis of each research scheme under different pump distances. From the table, it can be seen that with the increasing distance between the pump centers, the axial flow uniformity of section 2-2 also gradually increases, and the efficiency of the device also gradually increases, with a small change in head. In scheme 8, the axial flow uniformity at section 2-3 reaches 76.63%, and the head and hydraulic loss increase significantly, with little change in the efficiency of the device.

Table 5. CFD performance analysis of the research program.

Plan	Distance of Pump ( $D_I/D_S$ )	Head (m)	Efficiency (%)	Loss of Hydraulic (mm)
5	1.00	4.709	66.32	0.471
6	1.50	4.712	67.90	0.471
7	2.00	4.711	68.71	0.471
8	2.33	4.754	68.80	0.475

Figure 23 shows the axial flow velocity distribution on the multi-axis line of the suction sump. As can be seen from the figure, in program 5, the overall flow velocity distribution is more uniform, and the overall presentation of the two sides of the small middle large. In program 6, the two sides of the axial flow velocity distribution is significantly larger. In program 7, the overall axial flow velocity uniformity distribution is better. In program 8, line 1–4 axial line overall axial flow velocity distribution is more uniform, the peak is significantly lower, and the change is smaller.



**Figure 23.** Suction sump multi-axis on the axial flow velocity distribution with different arrangement spacing.

#### 4. Conclusions

- (1) Under the different installation speakers dangling height, when the water pump installation speakers impending height is greater than  $0.60 D_d$ , into the pool overall internal pressure distribution is more uniform, but there are vortex pump trumpet nozzle distribution, velocity uniformity of section 2-3 is relatively low, the device efficiency is relatively low, the distribution of the amount of swirl before the trumpet nozzle can also increase, the vortex quantity under the horn nozzle is connected with the bottom of the pump after entering, and the axial flow velocity between the surface layer and the bottom of the nozzle is relatively low, and the overall axial flow velocity distribution is not uniform. When the pump installation suspension height is  $0.8 D_d$ ,

the overall pressure distribution in the inlet pool decreases, the vortex disappears at the pump horn nozzle, the flow velocity uniformity at section 2-3 increases, and the device efficiency also increases. When the pump installation height is  $1.7 D_d$ , the pressure and streamline in the inlet pool have no obvious distribution change, but the vorticity near the horn nozzle has no obvious effect on the bottom of the inlet pool. When the pump installation height is  $0.8 D_d$ , it has an obvious influence on the flow velocity of the surface layer into the pool and has a great influence on the axial flow velocity and streamline distribution of the surface layer.

- (2) Under different pump spacings, when the pump spacing is  $1.00 D_s$ , the uniformity of the flow velocity at section 2-3 and the efficiency of the device is low, and the vorticity distribution in front of the horn nozzle is denser, presenting a group distribution. The reverse axial flow velocity distribution area behind the horn nozzle is larger, and the pressure distribution in the whole area below the horn nozzle is larger. When the pump spacing is  $1.50 D_s$ , the pump efficiency and flow velocity uniformity at section 2-3 increase, the vorticity distribution in front of the horn nozzle is no longer concentrated, and the reverse axial flow velocity distribution area behind the horn nozzle decreases and presents a small regional distribution. When the pump spacing is  $2.00 D_s$ , the device efficiency and flow velocity uniformity at section 2-3 continue to improve, the overall vorticity distribution near the horn nozzle does not change significantly, and the pressure distribution in the inlet pool decreases significantly. When pump spacing of  $2.33 D_s$  and pump assembly efficiency and uniformity section 2-3 flow to further improve, horn near the nozzle bigger pressure distribution area has increased, after the trumpet nozzle and trumpet nozzle side wall significantly reverse axial velocity, is in a good streamline distribution, plant efficiency change much, hydraulic loss relative increase.
- (3) To sum up, the recommended pump installation height is  $0.8 D_d$ , the maximum value of pump station design specification; in dual-pump mode, the recommended pump spacing is  $2.00 D_s$ .

**Author Contributions:** Data curation, S.L. (Songbai Li) and C.S.; Formal analysis, T.S. and C.Z.; Methodology, S.L. (Shuaihao Lei) and C.X.; Writing—original draft, S.L. (Shuaihao Lei); Writing—review and editing, L.C.; Supervision, L.C. All authors have read and agreed to the published version of the manuscript.

**Funding:** This research was funded by the National Natural Science Foundation of China (grant no. 51779214), A Project Funded by the Priority Academic Program Development of Jiangsu Higher Education Institutions (PAPD), the Key Project of Water Conservancy in Jiangsu Province (grant no. 2020030 and 2020027), and the Jiangsu Province South-North Water Transfer Technology Research and Development Project (SSY-JS-2020-F-45).

**Institutional Review Board Statement:** Not applicable.

**Informed Consent Statement:** Not applicable.

**Data Availability Statement:** Not applicable.

**Conflicts of Interest:** The authors declare no conflict of interest.

## Nomenclature

$\rho$	Fluid density
$u$	Speed vector
$\tau$	Stress Tensor
$F$	Volume force vector of fluid
$k$	Turbulent kinetic energy
$t$	Time
$u_i$	The velocity component of the fluid in the i-direction

$x_i, x_j$	Three-dimensional coordinate components
$\mu$	Dynamic viscosity of the fluid
$\mu_t$	Turbulent viscosity
$\sigma_k$	The Prandtl number corresponding to the turbulent kinetic energy $k$ , $\sigma_k = 1.0$
$G_k$	The term for the generation of turbulent kinetic energy $k$ caused by the mean velocity gradient
$G_b$	The term for the generation of turbulent kinetic energy $k$ caused by buoyancy
$\varepsilon$	Dissipation rate
$\sigma_\varepsilon$	Prandtl number corresponding to dissipation rate $\varepsilon$ , $\sigma_\varepsilon = 1.3$
$C_{1\varepsilon}, C_{2\varepsilon}, C_{3\varepsilon}$	Empirical constants, $C_{1\varepsilon} = 1.44$ , $C_{2\varepsilon} = 1.92$ , $C_{3\varepsilon} = 1.0$
$S_k, S_\varepsilon$	User-defined source items
$D_d$	Inlet flare diameter under single pump condition
$D_s$	Inlet flare diameter under double pumps condition
$D$	Impeller diameter
$D_h$	Overhang height
$D_l$	Layout spacing
$H$	Water level height in inlet sump
$H_i$	Height of the horizontal feature section relative to the bottom of inlet sump
$L$	Inlet sump length
$L_i$	Distance of longitudinal characteristic section relative to the gate
$V_u$	Axial flow uniformity
$u_{ai}$	Axial velocity of each node in the section
$u_a$	Average axial velocity of the section
$n$	Nodes
$h$	Hydraulic loss
$\Delta p$	Difference of total pressure between sections
$g$	Gravitational acceleration
$H_s$	Head
$P_{inlet}$	Inlet total pressure
$P_{outlet}$	Outlet total pressure
$\eta$	Efficiency
$Q$	Flow rate
$T$	Torque
$\omega$	angular velocity of impeller

### Abbreviations

CFD	Computational fluid dynamics
-----	------------------------------

### References

- Luo, C.; Lei, S.H.; Chen, F.; Liu, H.; Cheng, L. Numerical simulation of rectifying characteristics of the airfoil deflectors in the sump of pumping station. *J. Adv. Sci. Technol. Water* **2021**, *41*, 53–59.
- Feng, J.G.; Meng, X.Y.; Qian, S.T. Sill rectification characteristics downstream a unilaterally arranged pump-gateway. *J. Adv. Sci. Technol. Water* **2019**, *39*, 62–67.
- Gao, C. Study on the Influence of Diversion Pier on the Hydraulic Characteristics of Xifeihe Combined-Sluice Pump Project. Master's Thesis, Yangzhou University, Yangzhou, China, 2018.
- Wang, F.C. Study on the Hydraulic Characteristics of the Bidirectional Operation of the Sluice Station. Master's Thesis, Yangzhou University, Yangzhou, China, 2016.
- Tastan, K. Effects of Inlet Geometry on the Occurrence of a Free-Surface Vortex. *J. Hydraul. Eng.* **2018**, *144*, 04018009.1–04018009.11. [[CrossRef](#)]
- Huang, X.B.; Guo, Q.; Qiu, B.Y. Numerical Simulation of Air-entrained Vortex in Intake Based on Three-equation VLES Model. *J. Trans. Chin. Soc. Agric. Mach.* **2022**, *53*, 183–188.
- Tang, L. CFD Study on Influent Flow State Improvement of Qiqiaoweng Pumping Station in Nanjing. Master's Thesis, Yangzhou University, Yangzhou, China, 2019.
- Zi, D.; Wang, F.J.; Yao, Z.F.; Hou, Y.K.; Xiao, R.F.; He, C.L.; Yang, E.B. Effects analysis on rectifying intake flow field for large scale pumping station with combined diversion piers. *J. Trans. Chin. Soc. Agric. Eng. Trans. CSAE* **2015**, *31*, 71–77.
- Tatsuaki, N. Solving the Problem of Sedimentation at the Inlet of pumping Station by using Submerged Diversion Piers. *J. Water Resources Water Eng.* **1993**, *42*, 89–90.

10. Wang, M. Research on Hydraulic Performance of the Prefabricated Pumping Station by CFD. Master's Thesis, Yangzhou University, Yangzhou, China, 2016.
11. Echavez, G.; McCann, E. An experimental study on the free surface vertical vortex. *J. Exp. Fluids* **2002**, *1*, 414–421. [[CrossRef](#)]
12. Choi, J.W.; Choi, Y.-D.; Kim, C.-G. Flow uniformity in a multi-intake pump sump model. *J. Mech. Sci. Technol.* **2010**, *24*, 1389–1400. [[CrossRef](#)]
13. Zhang, Y.; Wu, P. Design and Application of Gate Pump. *Urban Roads Bridges Flood Control* **2019**, *2*, 186–187+22–23.
14. Guo, M.; Chen, Z.M.; Lee, Y.; Choi, Y.D. Air Entrainment Flow Characteristics of Horizontal and Elbow Type Gate Pump-Sump Model. *J. KSFJ J. Fluid Mach.* **2019**, *22*, 54–61. [[CrossRef](#)]
15. Li, M.Y. Design and technical analysis of integrated pump gate. *J. Mech. Electr. Inf.* **2020**, *29*, 126–127.
16. Shen, Y.H.; Zhu, Z.Q. Research on Natural Vibration Characteristics of Pump-gate Combination Gate Structure Considering Fluid-structure Interaction. *J. China Rural Water Hydropower* **2021**, *2*, 13–17.
17. Shi, S.R.; Yan, G.H.; Dong, J.; Sun, Y.X. Safety and optimization of horizontal pump gates. *J. Vib. Shock* **2021**, *40*, 42–47.
18. Shi, S.R.; Yan, G.H.; Dong, J.; Yang, Y. Safety and Optimization of Vertical Pump Gate. *J. Vib. Meas. Diagn.* **2021**, *41*, 176–181+207.
19. GB/T 50265-2010; Ministry of Water Resources of the People's Republic of China. Pump Station Design Specification. China Planning Press: Beijing, China, 2011.